Thesis Paper - A Hierarchical Dual Ensemble Kalman Filter

William Cook

0.1 Abstract

Dynamic models that simulate processes across large geographic locations, such as hydrologic models, are often informed by empirical parameters that are distributed across a geographical area and segmented by geological features such as watersheds. These parameters may be referred to as spatially distributed parameters. Spatially distributed parameters are frequently spatially correlated and any techniques utilized in their calibration ideally incorporate existing spatial hierarchical relationships into their structure. In this paper, a parameter estimation method based on the Dual State Ensemble Kalman Filter called the Dual State Hierarchical Ensemble Kalman Filter (DSHKEnKF) is presented. This modified filter is innovative in that it allows parameters to be placed into a set of groups that are smoothed using hierarchical modeling techniques. The usability and effectiveness of this new technique is demonstrated by applying it to a rainfall-runoff model that simulates subcatchment-scale hydrologic processes and contains high dimensional spatially distributed empirical parameters.

Contents

Symbols

x^-	vector of states, pre-correction
x^+	vector of states, post-correction
y	vector of predicted states
θ^-	vector of parameters, pre-correction
θ^+	vector of parameters, post-correction
u	forcing data
z	vector of observed states

Chapter 1

Introduction

Utilizing sequential data assimilation techniques to filter the output of hydrologic models is an efficient way to correct and calibrate hydrologic models before and after their implementation in scientific studies or public projects [24], [21], [23]. Observations such as SWE (snow water equivalent), streamflow, and precipitation are collected on a daily basis across various geographic regions, allowing real time information to be dynamically ingested by the hydrologic model and inform present and future predictions. More accurate models allow hydrologists to better understand the past and predict the future, and the need to research optimal methods of hydrologic data assimilation has been recognized [30] and researched [16], [23]. Observed hydrologic data may allow models that output streamflow or SWE states, such as rainfall-runoff models, to undergo parameter estimation. Many empirical parameters exist in hydrologic models such as the HBV model to account for wildcard environmental attributes such as the temperature threshold for melting snow in a snowpack system [17], the percolation of water from the upper to the lower reservoir of a groundwater system [17], or the dispersion of a wave through a channel in a Muskingham-Cunge routing system [20]. These parameters are frequently correlated and can have more then one set of values that produce good results [11], [17]. Parameter estimation for rainfall-runoff models has been an active area of research [27],[28] and research has progressed into the 21'st century [21], [32], [23].

Models that ingest data sequentially can have their variables efficiently filtered

by a Kalman Filter, a sequential data assimilation algorithm. Kalman Filters only need the previous timestep's state estimate and covariance matrices to update the current timestep's state estimate and covariance matrices based on a new observed state. The original Kalman filter[14] was created to solve linear problems and more complicated implementations must be used to solve non-linear problems. The extended Kalman Filter[12] works for mildly non-linear systems but does not function optimally on strongly non-linear systems[19]. The Unscented Kalman Filter[13] is an improvement on the Extended Kalman Filter that allows for the filtering of highly non-linear systems. The Ensemble Kalman Filter[7], a predecessor to the Unscented Kalman Filter, filters non-linear systems by generating an 'ensemble' of model instances and adding unique noise to each instance's forcing data. The main advantage of this ensemble based approach is the EnKF's capacity to approximate the complete prosterior of a problem as opposed to the Bayesian approximation calculated through the Unscented Kalman Filter method. The substitution of the original Kalman Filter's error covarience matrix with an ensemble covariance matrix also allows for the efficient computation of the covariance of high dimensional state vectors.

To calibrate model parameters as well as model states a Dual State Kalman Filter may be used as demonstrated by Moradkhani et. al in 2005 [21]. Dual state Kalman filters add a small perturbation to a series of parameters that the user wishes to calibrate. These perturbed parameters vectors are then corrected in a similar fashion to the state vectors. After this happens a second filter is run to correct the state vectors in the traditional fashion. The Dual State Ensemble Kalman Filter implemented by Moradkhani et. al[21] extends the Ensemble Kalman Filter into a dual state configuration and is shown to successfully predict a set of parameters.

An alternative method of parameter estimation that utilizes the Kalman Filter is the Joint Kalman Filter, which combines states and parameters into one vector that is calculated simultaneously without the need for a second run. Joint Ensemble Kalman Filters have been successfully implemented on hydrologic models [31], [36] and other models [5], but Joint Ensemble Kalman filters can suffer from "filter inbreeding" under certain circumstances [10] and introduce inconsistency in especially heterogeneous

formations [34]. Overall Dual Ensemble Kalman Filters have been shown to produce more accurate parameter estimations then Joint Ensemble Kalman Filters, especially in noisy situations or non-linear environments, with the major drawback of the Dual approach being its larger draw on computational power [18].

In this paper hierarchical modeling techniques are integrated into the Dual State Ensemble Kalman Filter's parameter perturbation equation to create a Hierarchical Dual State Ensemble Kalman Filter. A hierarchical parameter perturbation framework allows the model to account for parameters that are potentially hierarchically related. For example, the celerity being calculated for a series of subbasins may be hierarchically related to each other because of a larger watershed or geological feature enveloping them. To examine the Dual State Hierarchical Ensemble Kalman Filter's application to high dimensional spatially distributed raster data and geographical data the hydrologic model, a variation of a rainfall-runoff model, is implemented to predict streamflows across the state of Montana. The hydrologic model is informed by a variety of sub-components featuring high dimensional spatially distributed parameters, including a snowpack process, soil process, and a Muskingham-Cunge routing component. The hydrologic model's parameters can be linked to individual sub-basins with can in turn be sorted into hydrologic unit code watershed boundaries (HUC-4 watersheds). Accordingly, a Dual State Hierarchical Ensemble Kalman Filter is an good choice to calibrate this raster data because 1) the DSHKEnKF does not have to compute the high dimensional state covariance matrix during the update phase as the ensemble covariance matrix may be substituted in its place, 2) the hydrologic model is a sequential model that could conceivably benefit from real-time parameter correction, and 3) 10+ years of observed streamflow and SWE data may be compared to model data to test for over-fitting.

Chapter 2 covers the methods behind the Dual State Hierarchical Ensemble Kalman Filtering algorithm. Chapter 3 discusses the hydrologic model and how a Dual State Hierarchical Ensemble Kalman Filter was applied to it. Chapter 4 discusses results while Chapter 5 compares those results with calibrated parameters from a Dual State Ensemble Kalman Filter as implemented by Moradkhani et al 2005.

Chapter 2

The Hierarchical Dual Ensemble Kalman Filter Method

2.1 General Dynamic Model and Observations

A generic dynamic model can be defined as one more more discrete nonlinear stochastic processes[5]:

$$\mathbf{x_{t+1}} = f(\mathbf{x_t}, \mathbf{u_t}, \theta_\mathbf{t}) + \varepsilon_\mathbf{t} \tag{2.1}$$

where $\mathbf{x_t}$ is an n dimensional vector representing the state variables of the model at time step $\mathbf{t}$, $\mathbf{u_t}$ is a vector of forcing data (e.g temperature or precipitation) at time step $\mathbf{t}$, and $\theta_\mathbf{t}$ is a vector of model parameters which may or may not change per time step (e.g soil beta - β or degree day factor - DDF). The non-linear function f takes these variables as inputs and returns the updated state vector at the next timestep $\mathbf{x_{t+1}}$. The noise variable $\varepsilon_\mathbf{t}$ accounts for both model structural error and for any uncertainty in the forcing data.

A state's observation vector $\mathbf{z_t}$ can be defined as

$$\mathbf{z_t} = h(\mathbf{x_t}, \theta_\mathbf{t}) + \delta_\mathbf{t} \tag{2.2}$$

Where the $\mathbf{x_t}$ vector represents the true state, $\theta_\mathbf{t}$ represents the true parameters,

$h(.)$ is a function that determines the relationship between observation and state vectors, and $\delta_\mathbf{t}$ represents observation error. $\delta_\mathbf{t}$ is Gaussian and independent of $\varepsilon_\mathbf{t}$.

The Dual Hierarchical State Ensemble Kalman Filter can be split into three subsections: The prediction phase, the parameter correction phase, and the state correction phase.

2.2   DEnHKF Method

2.2.1   Prediction Phase

Just as in a standard Dual Ensemble Kalman filter [21], each ensemble member $\mathbf{i}$ is represented by a stochastic model similar to (2.1). The modified equation is as follows:

$$\mathbf{x_{t+1}^{i-}} = f(\mathbf{x_t^{i+}}, \mathbf{u_t^i}, \theta_\mathbf{t}^{\mathbf{i}-}) + \omega_\mathbf{t}, \quad \mathbf{i} = 1, ..., n \tag{2.3}$$

Where n is the total number of ensembles. The $-/+$ superscripts denote filtered $(+)$ and uncorrected $(-)$ values. Note that $\theta_\mathbf{t}^{\mathbf{i}-}$'s $\mathbf{t}$ subscript does not necessarily denote that θ is time dependent when implemented in the standalone model but rather indicates that parameter values change as they are filtered over time. The noise term ω_t accounts for model error and will hereafter be excluded from the state equation since all error is included in forcing data, see below [8].

Errors in the model design and process noise are accounted for through the perturbation the forcing data vector $\mathbf{u_t}$ with random noise $\zeta_\mathbf{t}^\mathbf{i}$ to generate a unique vector $\mathbf{u_t^i}$ for each ensemble [21], [5]. ζ_t^i is drawn from a normal distribution with a covarience matrix $Q_\mathbf{t}^\mathbf{i}$.

$$\mathbf{u_{t+1}^i} = \mathbf{u_t} + \zeta_t^i, \quad \zeta_t^i \sim N(0, Q_t^i) \tag{2.4}$$

Parameter Perturbation

To generate the apriori parameters θ_{t+1}^{i-}, an evolution of the parameters similar to the evolution of the state variables must be implemented. Implementations of parameter evolution in [29] added a small perturbation sampled from $N(0, \Sigma_t^\theta)$, where Σ_t^θ represents the covariance matrix of θ at timestep t. This legacy method of evolution resulted in overly dispersed parameter samples and the loss of continuity between two consecutive points in time [15] [5]. To overcome this the kernel smoothing technique developed by West [35] and implemented by Liu [15] has been used effectively in previous Dual Ensemble Kalman filter implementations [21] and similar models [5].

$$\theta_{t+1}^{i-} = a\theta_t^{i+} + (1-a)\bar{\theta}_t^+ + \tau_t^i \tag{2.5}$$

$$\tau_t^i = N(0, h^2 V_t) \tag{2.6}$$

Where $\bar{\theta}_t^+$ is the mean of the parameters with respect to the ensembles, $V_t = var(\theta_t^{i+})$, a is a shrinkage factor between $(0,1)$ of the kernel location, and h is a smoothing factor. h may be defined as $\sqrt{1-a^2}$. In previous research a values chosen between $(.45, .49)$ have been shown to be optimal [5], but note that h and a tend to vary per model and optimal values for these parameters are generally found via experimentation [21] [1] [2] [5].

Hierarchical Parameter Perturbation

In a standard hierarchical linear regression, a value y and its predictor variables α and β are contained in vectors $\mathbf{g_y}$, $\mathbf{g}_\alpha$, and $\mathbf{g}_\beta$ respectively, all of which are of size $N, j = 1, ..., n$. Vectors g_α and g_β have a mean and standard deviation of $\mu_\alpha, \sigma_\alpha$ and μ_β, σ_β respectively.

$$y_{j,g} = \alpha_g x_{j,g} + \beta_g, \quad \alpha_g \sim N(\mu_\alpha, \sigma_\alpha), \quad \beta_g \sim N(\mu_\beta, \sigma_\beta) \tag{2.7}$$

where α and β are determined to be hierarchically related properties drawn from their respective normal distributions. For a simple overview of hierarchical models

refer to Osborne [22], while [9] is a more in-depth reference.

In a Hierarchical Duel Ensemble Kalman Filter, parameter perturbation has been modified to have properties of a hierarchical linear regressive system. First, members of θ are sorted into a series of group vectors G. Each member j of a group vector G_g, where g is the specific group number, is related to other members through shared hierarchical characteristics (spatial or otherwise.) Algorithms (2.5) and (2.6) are then updated to conform to the hierarchical structure described in (2.7):

$$\theta^{\mathbf{i-}}_{\mathbf{t+1,g}} = aG^i_{t,g} + (1-a)\bar{\theta}^{+}_{\mathbf{t,g}} + \tau^{\mathbf{i}}_{\mathbf{t,g}} \tag{2.8}$$

$$G^i_{t,g} = N(\mu_\theta, \sigma_\theta) \tag{2.9}$$

$$\tau^{\mathbf{i}}_{\mathbf{t}} = N(0, h^2 V^i_{t,g}) \tag{2.10}$$

Where $\bar{\bar{\theta}}^{\mathbf{i+}}_{\mathbf{t,g}}$ is the mean over all ensembles for all members of group g, μ_θ and σ_θ are the grand mean and grand standard deviation respectively of all ensembles and points in group $\theta^+_{\mathbf{t,g}}$ (for clarity, the calculation of the grand mean and grand standard deviation returns a scalar value for each), and $V_{g,t}$ is the variance matrix with respect to the ensembles of all members of group g.

2.2.2 Parameter Correction Phase

In an Ensemble Kalman Filter, observations are perturbed to reflect model error. To accomplish this n unique perturbations are created. Therefore, the variable $\mathbf{z}^{\mathbf{i}}_{\mathbf{t+1}}$ is defined as follows:

$$\mathbf{z}^{\mathbf{i}}_{\mathbf{t+1}} = \mathbf{z_{t+1}} + \eta^{\mathbf{i}}_{\mathbf{t+1}}, \quad \eta^{\mathbf{i}}_{\mathbf{t+1}} = N(0, R_{t+1}) \tag{2.11}$$

Where z_{t+1} is an observation vector defined by (2.2) and η^i_{t+1} is a random perturbation drawn from a normal distribution with covarience matrix R_{t+1}. A set of state predictions that can be related to the observations are generated by running the

14

apriori state vector through the function $h(.)$:

$$\hat{\mathbf{y}}^{\mathbf{i}}_{\mathbf{t+1}} = h(\mathbf{x}^{\mathbf{i-}}_{\mathbf{t+1}}, \theta^{\mathbf{i-}}_{\mathbf{t+1}}) \tag{2.12}$$

The parameter update equation is similar to the update equation of the linear Kalman filter $\mathbf{x}^+_{\mathbf{t}} = \mathbf{x}^-_{\mathbf{t}} + K_t(\mathbf{z}_{\mathbf{t}} - H\hat{\mathbf{x}}_{\mathbf{t}})$, with $\hat{\mathbf{y}}^{\mathbf{i}}_{\mathbf{t+1}}$ serving the same purpose as $H\hat{\mathbf{x}}_{\mathbf{t}}$. However, unlike the linear kalman filter, parameters are corrected in lieu of the states in the first correction phase:

$$\theta^{i+}_{t+1} = \theta^{i-}_{t+1} + K^{\theta}_{t+1}(z^i_{t+1} - \hat{y}^i_{t+1}) \tag{2.13}$$

To facilitate this, K^{θ}_{t+1} is defined as

$$K^{\theta}_{t+1} = \Sigma^{\theta,\hat{y}}_{t+1}(\Sigma^{\hat{y},\hat{y}}_{t+1} + R_{t+1})^{-1} \tag{2.14}$$

where $\Sigma^{\theta,\hat{y}}_{t+1}$ is the cross covariance of θ_{t+1} and $\hat{y}_{t+1}$, $\Sigma^{\hat{y},\hat{y}}_{t+1}$ is the covarience of $\hat{y}_{t+1}$, and R_{t+1} is the observation error matrix from (2.11).

2.2.3   State Correction Phase

After θ^{i+}_{t+1} has been calculated the model is run again (2.3) with the θ^{i+}_{t+1} replacing θ^{i-}_{t+1}.

$$x^{i-}_{t+1} = f(x^{i+}_t, u^i_t, \theta^{i+}_t), \quad i = 1, ..., n \tag{2.15}$$

After a new state vector is generated it is re-run through (2.12) with the new parameter vector:

$$\hat{y}^i_{t+1} = h(x^{i-}_{t+1}, \theta^{i+}_{t+1}) \tag{2.16}$$

The corrected state vector is then run through the state update equation

$$x^{i+}_{t+1} = x^{i-}_{t+1} + K^x_{t+1}(z^i_{t+1} - \hat{y}^i_{t+1}) \tag{2.17}$$

$$K_{t+1}^x = \Sigma_{t+1}^{x,\hat{y}}(\Sigma_{t+1}^{\hat{y},\hat{y}} + R_{t+1})^{-1} \qquad (2.18)$$

where $\Sigma_{t+1}^{x,\hat{y}}$ is the cross covariance of x_{t+1} and $\hat{y}_{t+1}$.

Chapter 3

Application of DEnHKF to Hydrologic Model

3.1   The Hydrologic Model

The hydrologic model is used to test the viability of the DEnHKF method.   The hydrologic model takes parameters related to streamflows and groundwater, precipitation, minimum daily temperatures, and maximum daily temperatures as inputs and outputs streamflow values along with some additional states such as the amount of water precipitated as snowfall (henceforth referred to as *SWE* or snow water equivalent.)   The hydrologic model was designed to be implemented in any geographic location. For this study it was utilized to model streamflows throughout the state of Montana.

Configuring the hydrologic model to model streamflows throughout Montana is advantageous because it allows for the calibration of a very large number of spatially distributed, high dimensional parameters. These parameters can be expected to vary

Table 3.1: States

State (x)	Purpose	Dimensions
streamflow	Streamflow (in cubic meters per second)	330 (nodes)
swe	Snow Water Equivalent (in mm^3)	45012 (pixels)

Table 3.2: Forcing Data

Forcing Data (u)	Purpose	Dimensions
tempmin	Lowest temperature for timestep	45012 (pixels)
tempmax	Highest temperature for timestep	45012 (pixels)
precipitation	Amount of rainfall for timestep	45012 (pixels)

significantly across the entirety of Montana, a state which covers an area of 380,800 km^2 and sports diverse terrain.

3.1.1 Input Data

The hydrologic model takes rasterized precipitation data and temperature data from meteorological databases as input. This data can be utilized as a vector forcing data in the ensemble kalman filter framework (e.g: $u_t = [precip_t, Tmin_t, Tmax_t]$.)

3.1.2 Calibrated Parameters

The hydrologic model utilizes a HBV rainfall-runoff component and a Muskingum-Cunge routing component. The HBV component includes a precipitation and snow-pack process that utilizes the empirical parameters *degree day factor* ($\mathrm{mm°C^{-1}d^{-1}}$) and *temperature threshold* (°C), a soil process that utilizes the empirical parameters *potential evapo-transpiration* (dimensionless), *soil beta* (dimensionless), and *soil max water content* (mm), and a runoff generation process that utilizes the empirical parameters $ck0$ ($\mathrm{d^{-1}}$), $ck1$ ($\mathrm{d^{-1}}$), $ck2$ ($\mathrm{d^{-1}}$), $hl1$ (mm), and *perc* (d), all of which control various aspects of groundwater percolation and runoff. The Muskingum-Cunge routing component utilizes parameters that control *wave dispersion* (dimensionless) and *wave celerity* (seconds). To learn more about the hydrologic model, its algorithms, and the parameters that control it refer to Appendix A.

3.2 Observation Data

A Kalman Filter relies on one or more observed states for correction. Accordingly, observations were obtained for streamflows and snowfall across Montana. For stream-

Table 3.3: Calibrated Parameters

Parameter (θ)	Purpose
ddf	Degree Day Factor
aet_lp	Potential Evapo-Transpiration
soil_beta	Portion of ponded water that goes into soil storage
soil_max_wat	Soil compartment maximum water capacity
ck0	Immediate runoff
ck1	Fast runoff
ck2	Groundwater runoff
hl1	Groundwater water storage threshold
perc	Groundwater peculation
K	Wave celerity
e	Wave dispersion

Table 3.4: Observations

Observed State (x)	Source	Dimensions
streamflow	USGS	82
swe	NRCS	90

flow, USGS streamflow data was collected at 86 sites. Each observed site was paired with the closest simulated stream outlet within a 2.5 mile cutoff. For snowfall, SNOW-TEL sites monitored by the Natural Resources Conservation Service (NRCS) were used 3-1. 90 stations were chosen and matched to specific pixels in the hydrologic model's raster files.

3.3 Catchment Data and Hierarchical Groups

The hydrologic model utilizes the Watershed Boundary Dataset (WBD), a national hydrologic unit from the USGS that defines the areas of the United States landscape that drain to portions of the stream network, to separate Montana into 330 watersheds Fig. 3-2. Each watershed is associated with one of each type of parameter from Table 3.3. These 330 watersheds fall into 3 larger watershed zones (called HUC4, or 4-digit hydrologic unit boundaries) that were utilized to classify each watershed into one of 3 hierarchical zones Fig. 3-3.
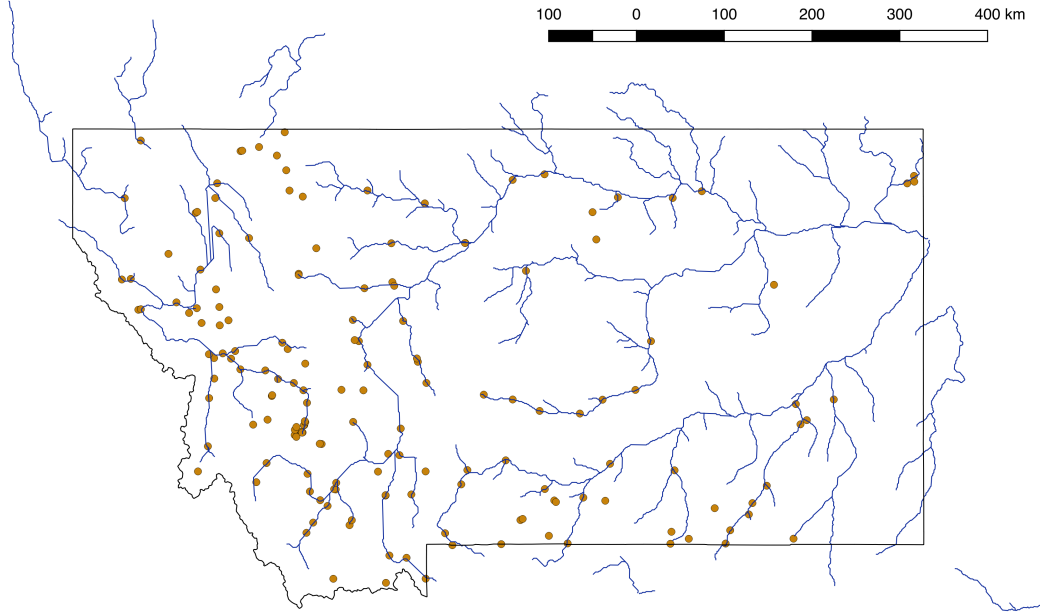
Figure 3-1: all SWE stations plotted against modeled streamflows

3.4   Filter Modifications

The DEnHKF filter was implemented with a series of modifications that streamlined the filtering process.

3.4.1   Parameter Ranges

Parameter minimums and maximums were implemented on each model parameter to avoid anomalous or erratic model output such as negative snowfall or streamflow. The use of parameter bounds in Kalman filters is well researched and they have been used in a variety of past studies [26].

For every parameter θ a minimum θ_{min} and a maximum value θ_{max} was defined. If an ensemble member i was generated outside of the range $(\theta_{min}, \theta_{max})$ during the apriori phase it was adjusted to:
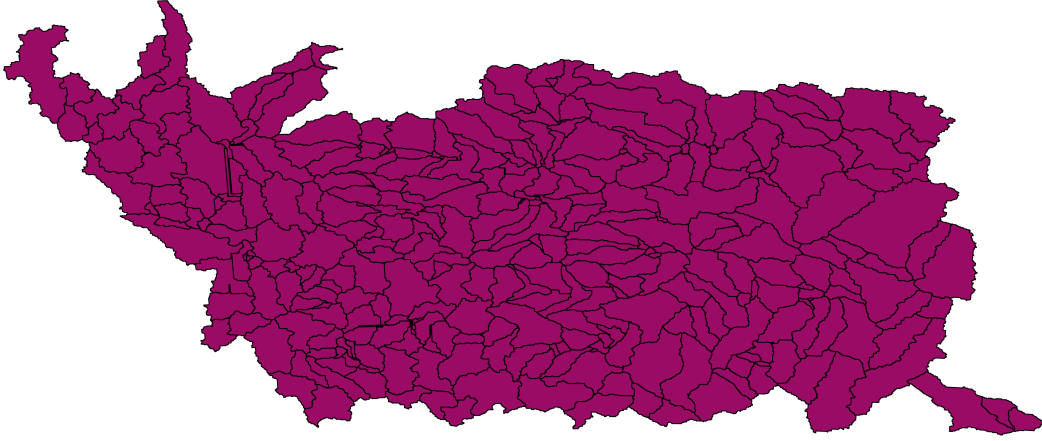
Figure 3-2: Subbasins - HUC8 polygons

$$\theta^i = \begin{cases} \theta_{min} & \theta^i < \theta_{min} \\ \theta_{max} & \theta^i > \theta_{max} \end{cases} \tag{3.1}$$

$$\theta^i = \begin{cases} \theta_{min} & \theta^i < \theta_{min} \\ \theta_{max} & \theta^i > \theta_{max} \end{cases} \tag{3.2}$$

For posterior parameters the same clipping logic from Eq. (3.2) is used. Initially an approach similar to the approach in [26] was utilized, but this logic kept parameters immobile when the innovation between the state and observations were very large, rendering the filter's parameter correction phase meaningless. To account for the problem of ensemble collapse, a minimum variance and a normalization feature was implemented (see below.)
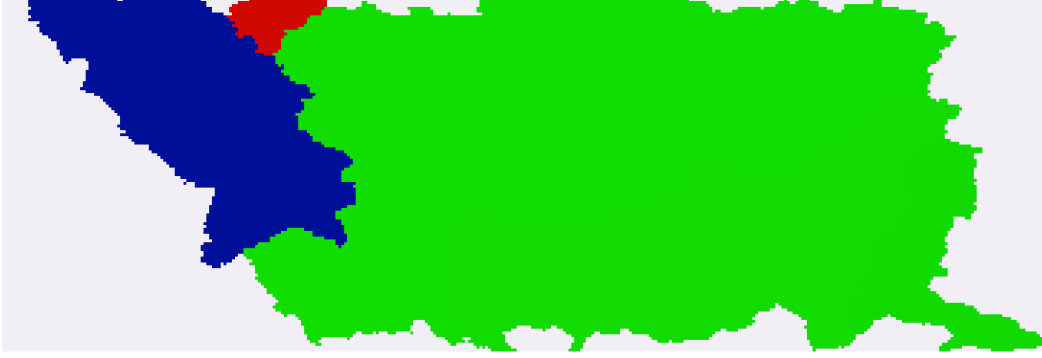
Figure 3-3: Montana's 3 HUC4 zones rendered onto the raster grid.

3.4.2   Normalization Feature

To reduce erratic parameter ensemble behavior when sudden large discrepancies between observed data and model data appeared, a normalization feature was implemented in the parameter correction phase. For every parameter parameter θ a maximum movement range θ_{range} was defined based upon boundaries θ_{min} and θ_{max}. An empirical parameter γ controlled the maximum amount of movement per correction phase.

$$\theta_{range} = \gamma(\theta_{max} - \theta_{min}) \tag{3.3}$$

$$\theta^+ = \begin{cases} \theta^+ & \theta^+ > \theta^- - \theta_{range}, \theta^+ < \theta^- + \theta_{range} \\ \theta^- - \theta_{range} & \theta^+ < \theta^- - \theta_{range} \\ \theta^- + \theta_{range} & \theta^+ > \theta^- + \theta_{range} \end{cases} \tag{3.4}$$

$\gamma = 1$ allows for unhindered movement for theta, while $\gamma = 0$ does not allow any movement. For the purposes of this paper $\gamma = .1$ greatly reduced filter instability while allowing parameters to converge relatively quickly to far away values.

3.5   Small Testset

A filtering run could take anywhere between 20 hours and a week depending on the date range and number of ensembles used. In order to efficiently test new equations and code additions a small 3 node dataset was developed. This dataset covered the Bitterroot area of Montana and only held 3 subbasins.

Chapter 4

Results

4.1   Perturation of States

Early attempts at running the DSHKEnKF on the hydrologic model were marked by the complete collapse of posterior ensemble covariance to the mean and erratic jumps from the minimum to the maximum bounds for all streamflow parameters. Snow water equivalent parameters and states, however, converged in a stable fashion. It was determined that these erratic jumps were due to the hydrologic model's dependence on the value of the catchments' lowest groundwater reservoir, an unobserved and uncorrected state, which was integral to the production of streamflow in each timestep. White noise added to the forcing data (precipitation and min/max temperature) was unable to generate adequately diverse ensemble behavior when groundwater states were uniform across ensembles. To account for this, perturbation of groundwater and streamflow states was implemented.

4.1.1   Perturbation of Groundwater States

The hydrologic model was extremely sensitive to its starting states, in particular the lower groundwater reservoir. A low groundwater would lead to underwhelming groundwater, incentivising the parameters `ck0`, `ck1`, and `ck2` to converge towards values that emptied all water pouring into the reservoirs so modeled streamflow could
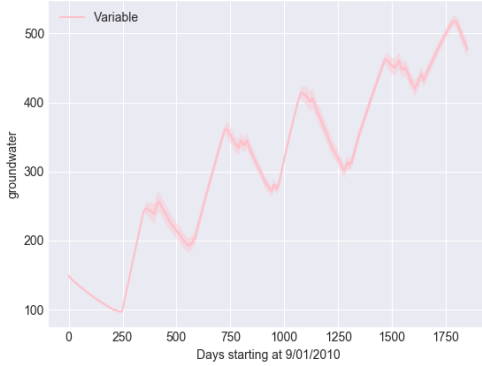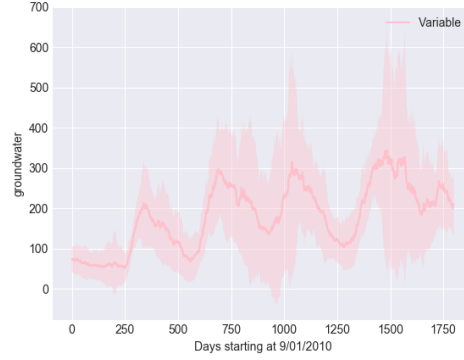
Figure 4-1: Uniform groundwater

Figure 4-2: Perturbed groundwater

match the observations. Conversely, high starting groundwater caused `ck0`, `ck1`, and `ck2` to converge towards parameters that let very little groundwater out of the reservoirs, further exasperating the problem and causing higher and higher values for `ck0`, `ck1`, and `ck2` to be chosen.

To solve this issue and find a reliable blanket starting value for groundwater subcatchments in an efficient amount of time the small dataset was utilized alongside the parameter boundaries specified by [17]. Trial and error was utilized on the dataset until groundwater stabilized. To encourage the model to explore different parameter values for different amounts of groundwater, initial states for the large dataset were perturbed across all ensembles and catchments using a μ equal to the average stable value of the small dataset, which for this model was roughly calculated to be 100mm, and a σ of 80mm. During the prediction phase groundwater was treated as forcing data and was perturbed slightly at a σ of $u_{gw} * gw$, with u_{gw} at .05

4.1.2 Continuous perturbation of streamflow and swe states

Another method of decoupling the model's calibration process from its over-reliance on groundwater was through the direct perturbation of streamflow and swe states. This perturbation guaranteed that ensemble collapse was never fully realized.
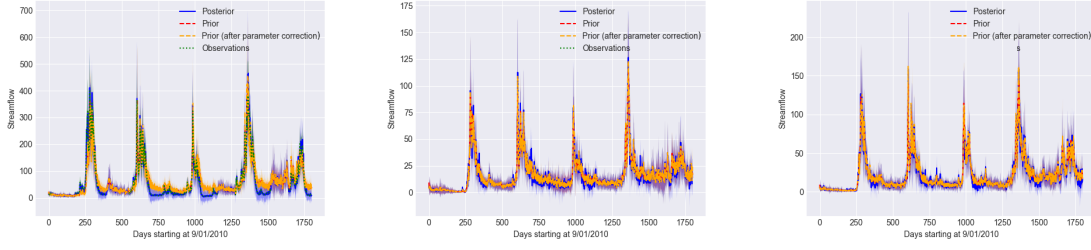
Figure 4-3: Streamflow states for the 3 catchments

4.2 Small dataset

To expedite the discovery of optimal initial values, errors, and minimum and maximum bounds for the complete dataset (see Table 4.1) the small dataset was run and compared with the ranges proposed by [25] and [33]. The small dataset, which was comprised of 3 catchments around the Biterroot valley and consisted of one gauged catchment (henceforth referred to as catchment 241) and 2 ungauged catchments (catchments 244 and 248), was run over a period of 1800 days, or a little under 5 years. Simulations began in September so modeled snowfall accumulation could be corrected first, allowing accurate snow melts to inform streamflow runoff in the Spring and Summer. All parameters in the small dataset converged to a set of values within the first 250-500 days and did not deviate significantly from those chosen values for the remainder of the filtering process.

4.2.1 Streamflow states and parameters

All 3 posterior streamflow states (Figure 4-3) snapped to the observations. The post-parameter correction streamflow (shown in yellow on the figures in 4-3) also followed the observations in the Spring and Summer time periods. Notice the discrepancy between the post parameter correction state and posterior state seen in the first graph in Figure 4-3 during the Winter time periods. While state correction continuously tried to move streamflow down to a match the observed Winter state, parameters were not found that allowed streamflow to match the observed states. This result is
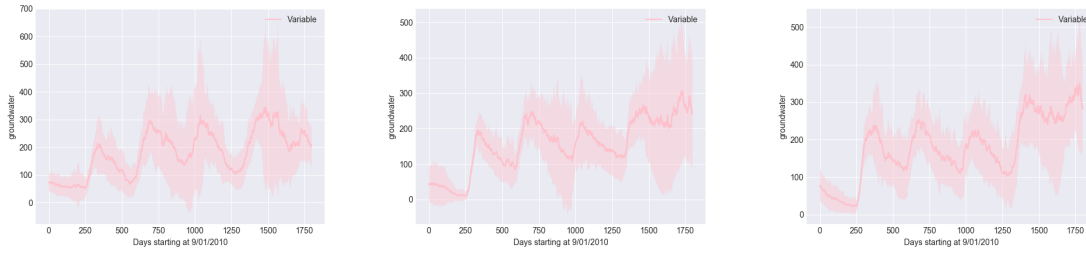
Figure 4-4: Groundwaters for the 3 catchments

connected to the behavior of the lower groundwater reservoir.

The lower groundwater reservoir in all three catchments rose 100mm-200mm throughout the 1800 day filtering period (Figure 4-4). Throughout this time the filter's values for ck2 and perc, two parameters that impact the buildup and dispersion of lower groundwater, remained unchanged. In this project, simulated groundwater was not compared to an observed state. Optimal groundwater behavior for the hydrologic model over long periods of time requires further research.

As seen in the plots in Figure **??**, parameter ensembles converged to the ensemble mean within the first 200-400 days. All catchments also converged to similar values. Since this is a predictable outcome for the small geographic area the small dataset encompasses, the large dataset is a better indicator of the effects of the hierarchical component upon the spatial independence of spatially distributed catchments.
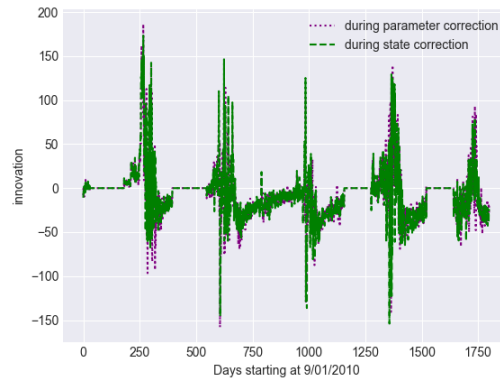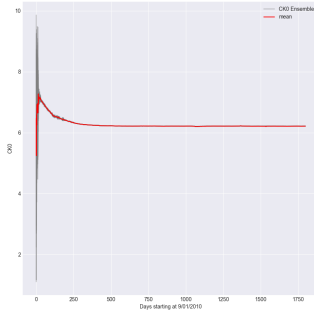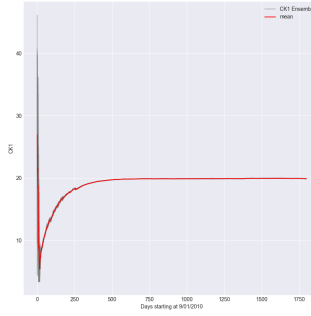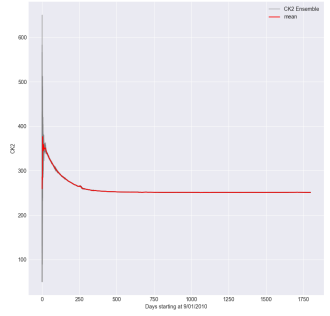

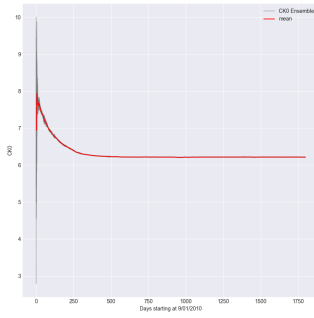Figure 4-5: Streamflow innovation (catchment 241)
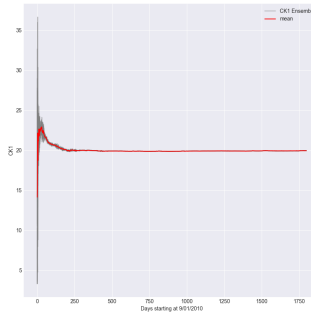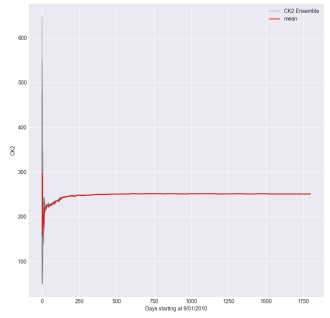
(a) 241:`ck0`   (b) 241:`ck1`   (c) 241:`ck2`

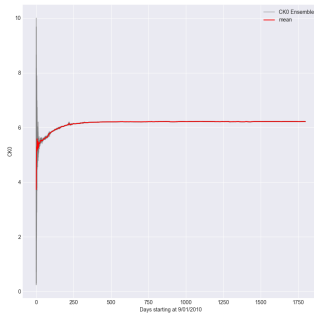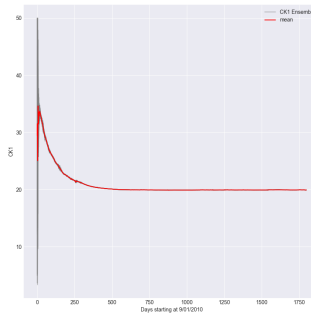(d) 244:`ck0`   (e) 244:`ck1`   (f) 244:`ck2`
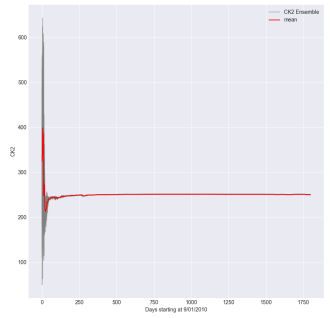
(g) 248:`ck0`   (h) 248:`ck1`   (i) 248:`ck2`

Figure 4-7: Convergence of `ck` parameters for all 3 catchments

29

Table 4.1: Hyperparameters - parameter perturbations and min/max ranges

Parameter (θ)	q	Min	Max
Degree Day Factor (`ddf`)	$.75\text{mm}°\text{C}^{-1}\text{d}^{-1}$	$1\text{mm}°\text{C}^{-1}\text{d}^{-1}$	$8\text{mm}°\text{C}^{-1}\text{d}^{-1}$
Tempature Threshold (`thres`)	$.5°\text{C}$	$-2.5°\text{C}$	$2.5°\text{C}$
Potential Evapo-Transpiration (`aet_lp`)	.15	.3	1
Ponded water to soil storage (`soil_beta`)	1.75	1	6
Soil compartment max capacity (`soil_max_wat`)	40	50mm	500mm
Immediate runoff (`ck0`)	6d^{-1}	$.25\text{d}^{-1}$	10d^{-1}
Fast runoff (`ck1`)	25d^{-1}	3.33d^{-1}	50d^{-1}
Groundwater runoff (`ck2`)	350d^{-1}	50d^{-1}	650d^{-1}
Groundwater water storage threshold (`hl1`)	25mm	0mm	50mm
Groundwater peculation (`perc`)	1.5d	3d	50d
Wave celerity (`K`)	82400	81576	84872
Wave dispersion (`e`)	.35	.25	.4
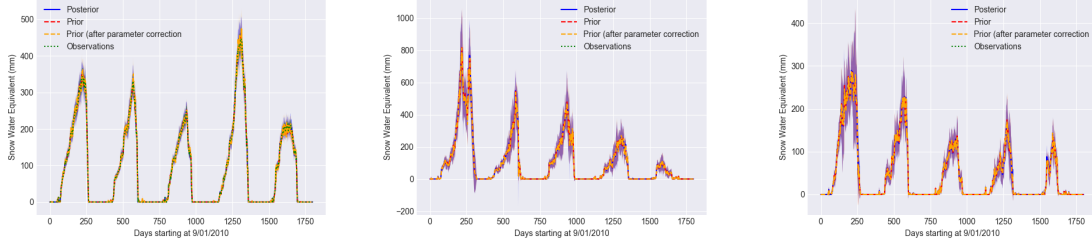
Figure 4-8: Snow-water equivalent states for the 3 catchments

4.2.2 Snow-water equivalent states and parameters

Snow-water equivalent states and parameters behaved similarly to their streamflow counterparts. Snow-water equivalent states (Figure 4-8) snapped to the observations quickly. Snow-water equivalent innovation (Figure 4-9) is much less biased then streamflow innovation (Figure 4-5). Snow-water equivalent parameters behaved similarly to their streamflow counterparts. All ensembles and catchments converged to a very similar value within the first 200-400 timesteps (Figure **??**.)

4.3 Complete Dataset

After workable initial values, errors, and boundaries and had been selected the complete dataset was calibarated. Calibration of the complete dataset was computation-
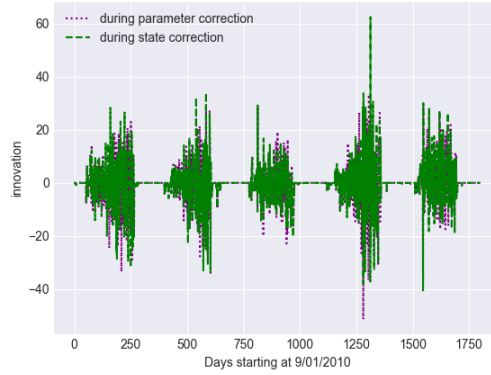
Figure 4-9: SWE innovation (catchment 241)

ally expensive and a balance had to be struck between ensemble size, time run, and data collected per timestep. For these results a full year (365 days) was run with 125 ensemble members. Running periods larger then one year came at the price of reducing the ensemble members, which led to unstable and unusable posterior corrections (Figure 4-20). Running the DSHKEnKF on the large dataset produced mixed results that point to both strengths in the hierarchical design and further research opportunities.

4.3.1 Streamflow states and parameters

Streamflow calibration on the large dataset proved to be a difficult process. While the posterior state vector matched the observations, innovation was heavily biased and both the prior and post-parameter correction prior had trouble locking onto parameters during the Summer months, resulting in an unstable prior and biased innovation (Figure 4-14.) This erratic behavior was more pronounced before it was reduced by the changes referenced in section 4.1. Unfortunately, these techniques could not be utilized to entirely balance the innovation since excessive state noise resulted in overly weak and unreliable parameter correction.

31
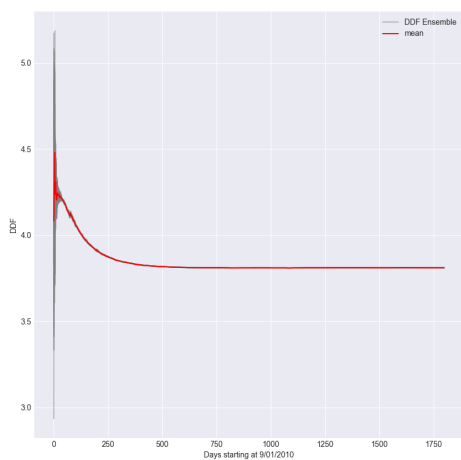
(a) 241:`ck0`
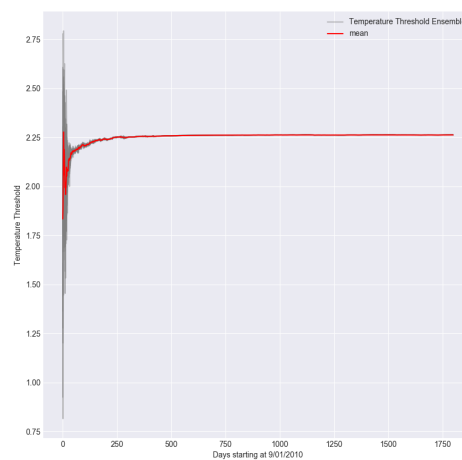
(b) 241:`ck2`
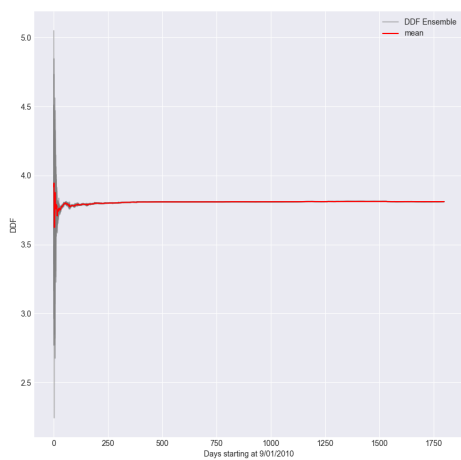
(c) 244:`ck0`
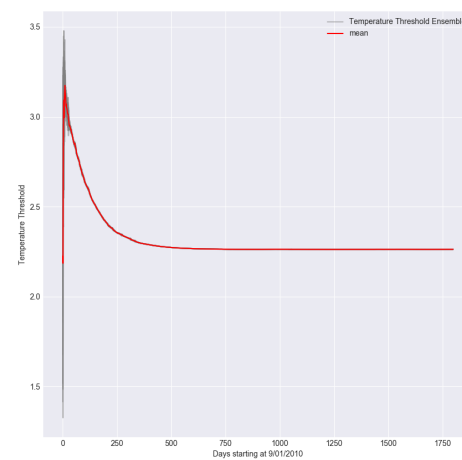
(d) 244:`ck2`
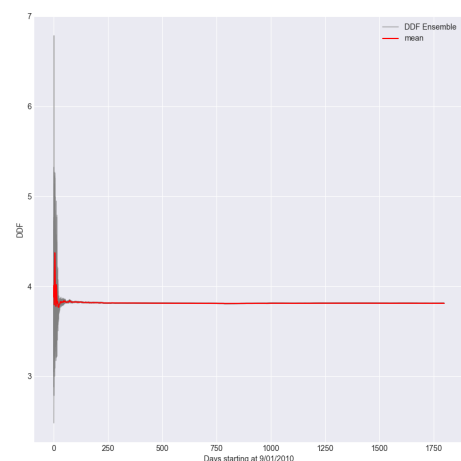
(e) 248:`ck0`
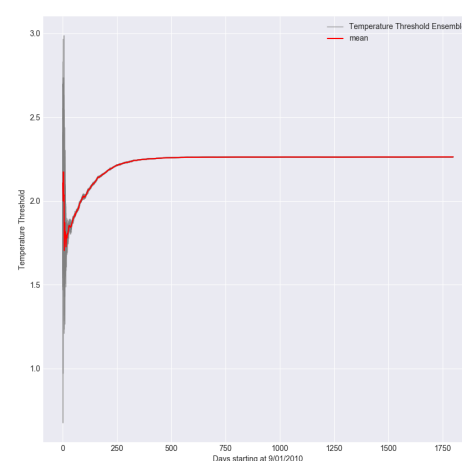
(f) 248:`ck1`

Figure 4-11: Convergence of `ck` parameters for all 3 catchments
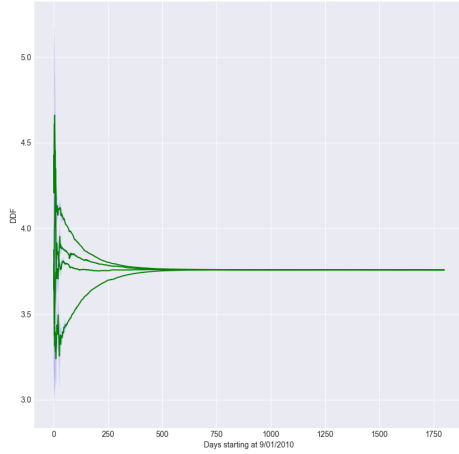
(a) All catchments:`ddf`
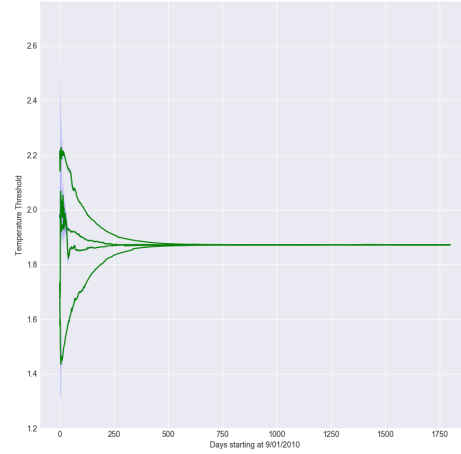
(b) All catchments:`pp`

Figure 4-13: All SWE parameters throughout the small dataset converged to a similar value. `a` blending value = .009
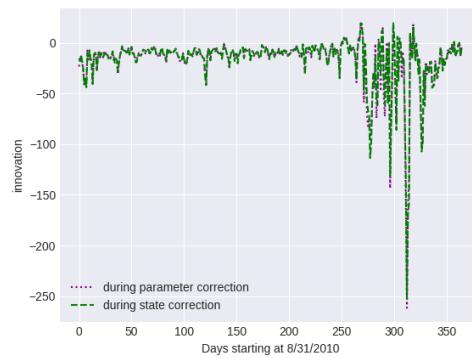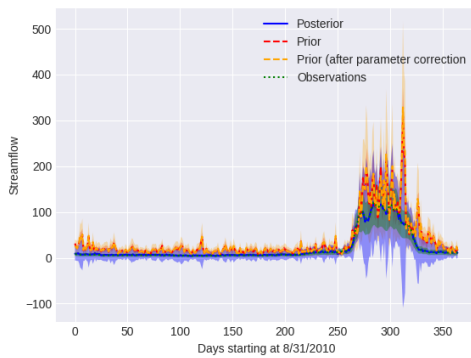
Figure 4-14: A gauged streamflow state and its innovation
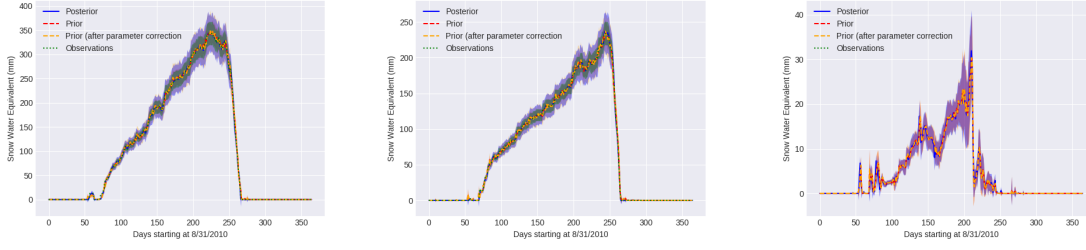
Figure 4-15: Snow-water equivalent states for 3 catchments: 241 (gauged), 302 (gauged), and 305 (ungauged)
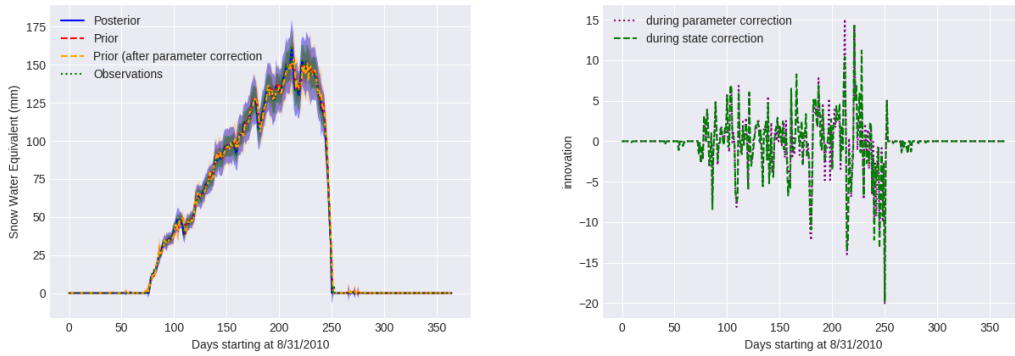
Figure 4-16: A gauged swe state and its innovation (catchment 193)

4.3.2 Snow-water equivalent states and parameters

Snow-water equivalent calibration on the large dataset was similar to the calibration of the small dataset and is a better demonstration of the successful calibration of a large-scale model component then streamflow calibration.

While `ddf` and `pp` were not run in a sufficient amount of time to stabilize to a value due to the aforementioned computational limitations, all catchments (Figure ??) are seen behaving in a similar fashion to their small dataset counterparts (Figure ??.)

4.4 Effects of the Hierarchical Blending Component

To observe the effects of the hierarchical component the small dataset was used.
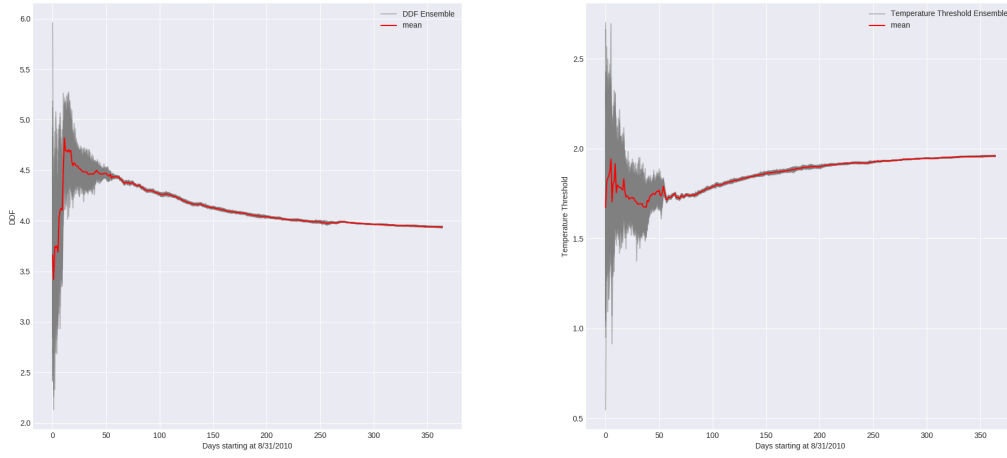
Figure 4-17: ddf and temperature threshold - catchment 193
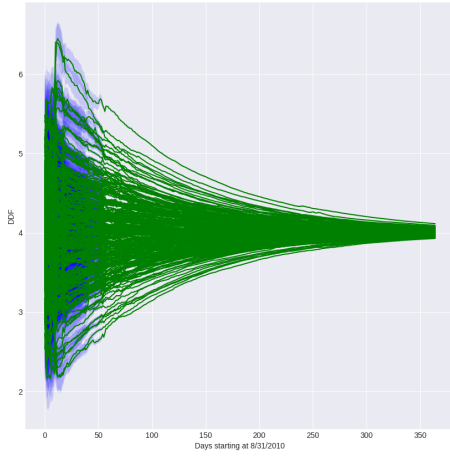
(a) Hierarchical Group 1:`ddf`
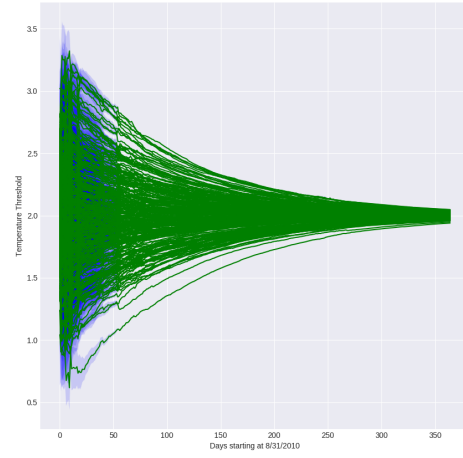
(b) Hierarchical Group 1:`pp`
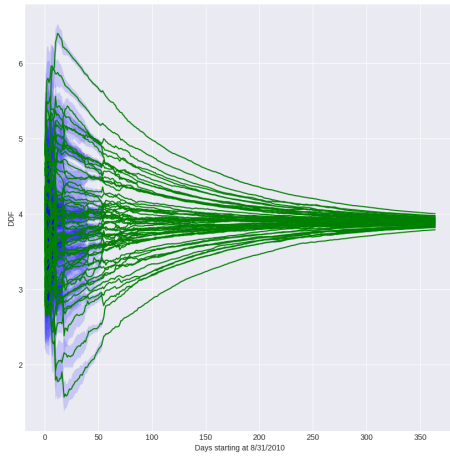
(c) Hierarchical Group 2:`ddf`
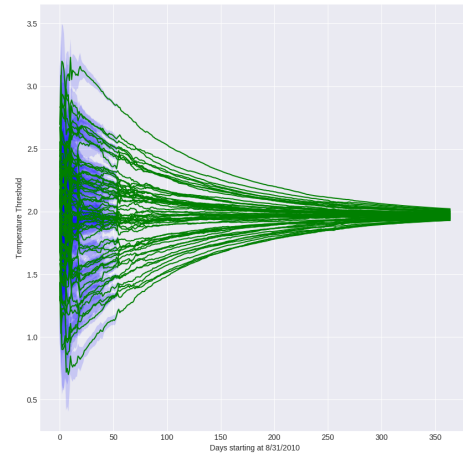
(d) Hierarchical Group 2:`pp`

Figure 4-19: All catchment parameters converging to a similar value. `a` blending value = .009
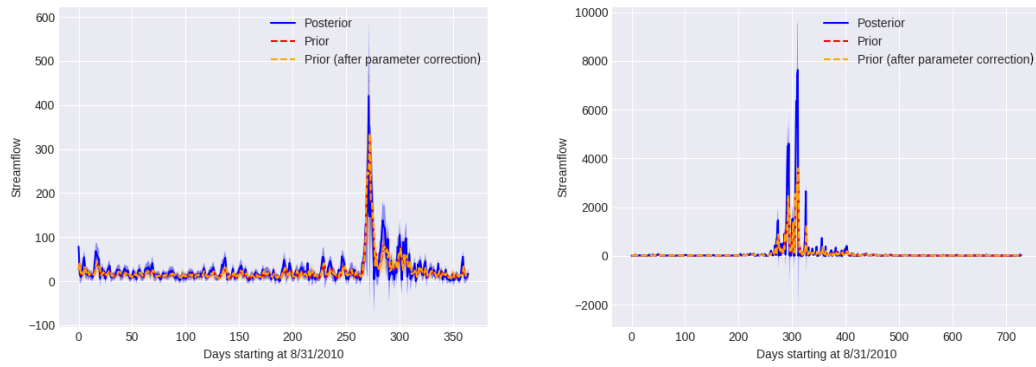
Figure 4-20: Ungaged catchment 327 - 125 ensemble members over 1 year (left) compared to 80 ensemble members over 2 years (right)

Appendix A

The Hydrologic Model

This model is a hydrologic system that couples a rainfall-runoff model to a routing component that simulates streamflows within a regional stream network. An HBV model [3, 4] was modified to simulate hydrologic processes like snowmelt, evapotranspiration, and infiltration at the subcatchment level and transform the resulting precipitation into runoff and streamflow. This streamflow is then routed via the Muskingum-Cunge routing algorithm [6]. Below is a description of the implementation of those algorithms.

A.0.1 Rainfall Runoff component

The HBV model [3, 4] contains a mixture of raster-based and vector-based operations. Raster-based operations utilize spatially distributed data drawn from meteorological databases (precipitation and temperature data.) The raster grid is also used to calculate snow accumulation, melt, and soil processes. These are informed both by input from the meteorological databases and by a series of spatially distributed parameters, such as potential evapotranspiration. Vector-based operations increase computational efficiency through the use of polygons. Unique polygons are indexed by k later in this appendix while grid points are indexed by j. Uniform hydrologic response units (HRUs) are implemented to aggregate runoff production over these polygons and thus act as the bridge between the vector based operations and raster

Table A.1: Hydrologic Model Outputs - Raster or Vector

Name	Category
Snow Water Equivalent	Raster
Evapo-Transpiration	Raster
Snow Melt	Raster
Pond	Raster
Soil Moisture	Raster
Upper Soil Storage	Vector
Lower Soil Storage	Vector
Runoff	Vector

based output. Table A.1 categorizes each model output as a vector based (one value per polygon) or raster-based (one value per pixel) output.

Precipitation/Snowpack   To determine the amount of precipitation that becomes snowfall and which amount becomes rainfall, minimum and maximum temperature data are compared to a critical temperature threshold Tc.

$$Snow_j^t = \begin{cases} P_j^t & Tmax_j^t < Tc_j \\ P_j^t * \frac{Tc_j - Tmin_j^t}{Tmax_j^t - Tmin_j^t} & Tmin_j^t < Tc_j < Tmax_j^t \\ 0 & Tmin_j^t > Tc_j \end{cases} \tag{A.1}$$

$$Rain_j^t = P_j^t - Snow_j^t \tag{A.2}$$

Where variables and parameters with a subscript j are spatially distributed and are at unique gridpoint j and variables and parameters with a superscript t are time-dynamic. P is precipitation ($\mathrm{mm\,d^{-1}}$), $Tmax$ is maximum air temperature (°C), $Tmin$ is minimum air temperature, $Snow$ is precipitation as snowfall ($\mathrm{mm\,d^{-1}}$), and $Rain$ is liquid precipitation. Any snowfall during one day t contributes to the snowpack's snow water equivalent (SWE, (mm)):

$$SWE_i^t = SWE_i^{t-1} + Snow_j^t \Delta t \tag{A.3}$$

A degree day model is utilized to simulate snowpack melt. Snowpack begins to

melt when the average air temperature exceeds air temperature threshold Tm.

$$Melt_j^t = ddf_j * (Tav_j^t - Tm_j)] \text{ for } Tav_j^t > Tm_j \tag{A.4}$$

$$Rain_j^t = P_j^t - Snow_j^t \tag{A.5}$$

Where $Melt$ represents water released from the snowpack $(\mathrm{mm\,d^{-1}})$, Tav is average air temperature over the time step $(°\mathrm{C})$, and ddf is the degree day factor $(\mathrm{mm\,d^{-1}\,°C^{-1}})$. ddf is an empirical parameter controlling the snowmelt rate per degree of air temperature above temperature threshold Tm.

Melt from the snowpack at time t is subtracted from the snowpack and added to the amount of ponded water:

$$Pond_j^t = Pond_j^{t-1} + (Melt_j^t + Rain_j^t)\Delta t \tag{A.6}$$

$$SWE_j^t = SWE_j^t - Melt_j^t\Delta t \tag{A.7}$$

Where $Pond$ (mm) represents liquid water ponding at the surface.

Soil processes   Ponded water either infiltrates into the soil and is either placed in the soil system or is added to the topsoil compartment where it generates speedy runoff. The fraction of ponded water that infiltrates is an exponential function of the relative water storage already in the soil:

$$\Delta SM_j^t = Pond_j^t * \left(1 - \frac{SM_j^t}{FC_j^t}\right)^\beta \tag{A.8}$$

$$\tag{A.9}$$

where SM (mm) is the amount of water in the soil compartment and FC (mm) is the maximum capacity of water the soil compartment can hold before water begins per-

colating to the groundwater system. *beta* (dimensionless) is an empirical parameter. Actual evapotranspiration (AET, $\mathrm{mm\,d^{-1}}$) is calculated at the same time. Actual evapotranspiration reduces the amount of water storage in the soil and, just like ΔSM_j^t, is informed by the degree of saturation in the soil (SM over FC).

$$AET_j^t = PET_j^t * \left(\frac{SM_j^t}{FC_j * LP_j} \right)^l \tag{A.10}$$

$$\tag{A.11}$$

where PET is potential evapotranspiration ($\mathrm{mm\,d^{-1}}$)) and l (dimensionless) is an empirical parameter. Soil water storage dynamics and the amount of surface water that generates fast runoff are controlled by infiltration and actual evapotranspiration:

$$SM_j^t = SM_j^t + \Delta SM_j^t - AET_j^t \Delta t \tag{A.12}$$

$$OVL_j^t = Pond_j^t - \Delta SM_j^t \tag{A.13}$$

where OVL (mm) represents water that recharges the near-surface runoff-generating compartment.

Groundwater Compartments and runoff generation   The groundwater system is comprised of two ground-water compartments that generate outflow. The top compartment's outflow represents both immediate runoff and fast runoff. The lower compartment's outflow represents baseflow. These processes are performed at the HRU level, which means that overland flow and soil moisture values, both of which are represented over the raster grid, are averaged over overlaid polygonal subwatersheds representing HRUs. Spatial arithmetic that averages soil water storage over all grid cells j contained within a given polygonal HRU k is indicated by angle brackets $< . >$. The mass balance and percolation of water from the upper to the lower compartment of the groundwater system is implemented as:

$$Rech_k^t = <OVL_j^t>_k + <max(SM_j^t - FC_j, 0)>_k \tag{A.14}$$

$$SUZ_k^t = SUZ_k^{t-1} + Rech_k^t + Pond_k^t - Q0_k^t \Delta t - Q1_k \Delta t - PERC_k \tag{A.15}$$

$$SLZ_k^t = SLZ_k^{t-1} + PERC_k - Q2\Delta t \tag{A.16}$$

$Rech$ (mm) represents water storage in the fast runoff generating near-surface compartment, SUZ (mm) represents the storage in the upper groundwater compartment, and SLZ (mm) represents water storage in the lower groundwater compartment in HRU k at time step t. $Q0$, $Q1$, and $Q2$ (mm d^{-1}) are each unique runoff rates. $Q0$ represents the soil surface runoff rate, $Q1$ represents the upper soil compartment runoff rate, and $Q2$ lower soil compartment runoff rate. These are calculated as follows:

$$Q0_k^t = max((SUZ_k - HL1_k) * \frac{1}{CK0_k}, 0.0) \tag{A.17}$$

$$Q1_k^t = SUZ_k * \frac{1}{CK1_k} \tag{A.18}$$

$$Q2_k^t = SLZ_k * \frac{1}{CK2_k} \tag{A.19}$$

$$Qall_k^t = Q0_k^t + Q1_k^t + Q2_k^t \tag{A.20}$$

$HL1$ (mm) is an empirical parameter controlling a water storage threshold that triggers the generation of fast runoff. $CK0$, $CK1$, and $CK2$ (d) are empirical parameters that represent the characteristic drainage times of the soil surface, upper compartment, and lower compartment respectively.

Total outflow from any given HRU k on day t is distributed over time in order to produce the catchment response. This is accomplished through the convolution the output of HRU k by triangular standard unit hydrograph with base M_{base}.

$$Q_j^t = \sum_{i=1}^{M_{base}} Qall_j^{t-i+1} U(i) \tag{A.21}$$

$$U(i) = \begin{cases} \frac{4}{M_{base}^2} * i & 0 < i < M_{base}/2 \\ -\frac{4}{M_{base}^2} * i + \frac{4}{M_{base}} & M_{base}/2 < i < M_{base} \end{cases} \tag{A.22}$$

where U is a triangular hydrograph of area 1 and a base integer $MAXBAS$ (d) representing the duration of the hydrograph.

A.0.2 Routing component

The runoff responses generated from each HRU are routed through the stream network via the Muskingum-Cunge routing model. Each stream reach k has a storage given by the proceeding discharge-storage equation.

$$S_k^t = K \left[eQ_{in} + (1-e)Q_{out} \right], \tag{A.23}$$

where K (d) and e (dimensionless) are empirical parameters controlling the celerity and dispersion of the wave routed through the channel respectively.

Substituting this relationship in a finite-difference form of the continuity equation $\frac{S_j^{t+1} - S_j^t}{\Delta t} = Q_{in} - Q_{out}$ for a multi-reach system with lateral inflows injected to the upstream of reach dreaming HRU j at an average constant rate through timestep t q_j^{t+1} results in:

$$Q_j^{t+1} \left[K_j(1-e_j) + 0.5\Delta t \right] + Q_{j-1}^{t+1} \left[K_j e_j - 0.5\Delta t \right] \tag{A.24}$$

$$= Q_j^t \left[K_j(1-e_j) - 0.5\Delta t \right] + Q_{j-1}^t \left[K_j e_j + 0.5\Delta t \right] \tag{A.25}$$

$$+ q_j^{t+1} \left[K_j(1-e_j) + 0.5\Delta t \right] \tag{A.26}$$

Each HRU contains one reach with an upstream and a downstream node. Stream-

flow reaches $j = 1, ..., J$ are integrated with respect to time using a first-order explicit finite difference scheme. The system of J equations can be assembled as a linear system of the form:

$$\mathbf{AQ^{t+1}} = \mathbf{B} \tag{A.27}$$

$\mathbf{Q^{t+1}}$ is a vector of unknown streamflows at time $t + 1$ solved each time step for every reach in J. The matrices $\mathbf{A}$ and $\mathbf{B}$ are functions of the model parameters and streamflows at t:

$$\mathbf{A} \equiv (\mathbf{a} + \mathbf{\Phi b})^T \tag{A.28}$$

$$\mathbf{B} \equiv (\mathbf{d} + \mathbf{\Phi c})^T \mathbf{Q}^t + \mathbf{I}(\mathbf{a} \odot \mathbf{q}^{t+1}) \tag{A.29}$$

where $\mathbf{\Phi}$ is a JxJ sparse connectivity (0,1)-matrix defining which pairs of nodes are connected. Flow direction is from row nodes to column nodes. All rows representing upstream nodes of $HRUs$ that drain an outlet node are zeros. Lastly:

$$\mathbf{a} = \mathbf{I}(\mathbf{K} - \mathbf{K} \odot \mathbf{e}) + dt * 0.5 \tag{A.30}$$

$$\mathbf{b} = \mathbf{I}(\mathbf{K} \odot \mathbf{e}) - dt * 0.5 \tag{A.31}$$

$$\mathbf{c} = \mathbf{I}(\mathbf{K} - \mathbf{K} \odot \mathbf{e}) - dt * 0.5) \tag{A.32}$$

$$\mathbf{d} = \mathbf{I}(\mathbf{K} \odot \mathbf{e}) + dt * 0.5 \tag{A.33}$$

$\mathbf{K}$ is an identity matrix of order J. e and $\mathbf{K}$ are column vectors holding parameters e and K for every reach in N. The $\odot$ operator denotes the Schur (elementwise) product between two vectors. The solution of (B.27) will become unstable if $\Delta t > 2 * K_j * (1 - e_j)$. To guard against this an an adaptive time stepping scheme was implemented. In this adaptive scheme the default timestep is reduced by an integer

45

fraction until the stability condition is satisfied for all reaches.

Appendix B

daWUAPhydroengine

REWRITE THIS

The hydrologic system is simulated using a rainfall-runoff model coupled to a routing component that simulates streamflows in the regional stream network. We adapted the HBV model [?, ?] to simulate subcatchment-scale hydrologic processes (snowmelt, evapotranspiration, infiltration) and to transform precipitation into runoff and streamflow. Runoff that reaches the channel is routed through the stream network using the Muskingum-Cunge routing algorithm [?]. In this appendix we provide here a description of the implementation of the algorithms.

B.0.1   Rainfall Runoff component

The HVB model [?, ?] is implemented as a mixture of gridded and vector-based operations to leverage the distributed nature of raster meteorological datasets while simultaneously taking advantage of the reduced computational burden of operating over polygons that aggregate runoff production over uniform hydrologic response units (HRUs).

Snowpack accumulation and melt and soil processes are calculated over the uniform raster grid imposed by the meteorological inputs (precipitation, air temperature, and potential evapotranspiration). In the next two paragraphs subscript i indicates that the variable or parameter is spatially distributed and is represented at grid point

i. Superscript t indicates that the variable is dynamic and its value is represented at time step t. Variables with no script or superscript indicate that the variable is spatially constant or time invariant.

Precipitation and snowpack processes Precipitation is partitioned between snowfall and rainfall using minimum and maximum daily air temperatures and a critical temperature threshold Tc that determines the the snow-rain transition:

$$Snow_i^t = \begin{cases} P_i^t & Tmax_i^t < Tc_i \\ P_i^t * \frac{Tc_i - Tmin_i^t}{Tmax_i^t - Tmin_i^t} & Tmin_i^t < Tc_i < Tmax_i^t \\ 0 & Tmin_i^t > Tc_i \end{cases} \tag{B.1}$$

$$Rain_i^t = P_i^t - Snow_i^t \tag{B.2}$$

where P is precipitation ($\mathrm{mm\,d^{-1}}$), T_{max} and T_{min} are maximum and minimum air temperature (°C), $Rain$ is liquid precipitation and $Snow$ is snowfall at pixel i during time step t ($\mathrm{mm\,d^{-1}}$). Snowfall during day t contributes to the snow water equivalent (SWE, (mm)) of the snowpack:

$$SWE_i^t = SWE_i^{t-1} + Snow_i^t \Delta t \tag{B.3}$$

The snowpack melt process is simulated using a degree day factor model occurs when average air temperature exceeds a air temperature threshold (Tm):

$$Melt_i^t = ddf_i * (Tav_i^t - Tm_i)] \text{ for } Tav_i^t > Tm_i \tag{B.4}$$

$$Rain_i^t = P_i^t - Snow_i^t \tag{B.5}$$

where $Melt$ is the amount of water output from the snowpack ($\mathrm{mm\,d^{-1}}$), Tav is average air temperature over the time step (°C), and ddf is the degree day factor ($\mathrm{mm\,d^{-1}\,°C^{-1}}$), an empirical parameter that represents the snowmelt rate per degree

of air temperature above Tm. Any melt form the snowpack during time t is subtracted from the snowpack storage (SWE) and added to the amount of water ponded in the surface:

$$Pond_i^t = Pond_i^{t-1} + (Melt_i^t + Rain_i^t)\Delta t \tag{B.6}$$

$$SWE_i^t = SWE_i^t - Melt_i^t \Delta t \tag{B.7}$$

where $Pond$ (mm) is liquid water available on the surface to infiltrate or produce runoff.

Soil processes Recharge into the soil system occurs when liquid water ponding the surface infiltrates into the soil. Ponded water that is not infiltrated increases the topsoil compartment that generates fast runoff. The fraction of ponded water that infiltrates into the soil is a exponential function of the relative water storage in the soil:

$$\Delta SM_i^t = Pond_i^t * \left(1 - \frac{SM_i^t}{FC_i^t}\right)^{\beta} \tag{B.8}$$

$$\tag{B.9}$$

where SM (mm) is the amount of water in the soil compartment, FC (mm) is the maximum amount of water soil can hold before water starts percolating to the groundwater system, and *beta* (dimensionless) is an empirical parameter. Simultaneously, actual evapotranspiration (AET, $\mathrm{mm\,d^{-1}}$) reduces the amount of water storage in the soil and is also controlled by the degree of saturation of the soil (ration of SM to FC).

$$AET_i^t = PET_i^t * \left(\frac{SM_i^t}{FC_i * LP_i} \right)^l \tag{B.10}$$

$$\tag{B.11}$$

where PET is potential evapotranspiration ($\mathrm{mm\,d^{-1}}$)) and l is an empirical dimensionless parameter. Infiltration and actual evapotranspiration control the dynamics of water storage in the soil and amount of surface water that generates fast runoff:

$$SM_i^t = SM_i^t + \Delta SM_i^t - AET_i^t \Delta t \tag{B.12}$$

$$OVL_i^t = Pond_i^t - \Delta SM_i^t \tag{B.13}$$

where OVL (mm) is water that recharges the upper (near-surface) runoff-generating compartment.

Percolation and runoff generation   Excess water in the topsoil and in two groundwater compartments generate outflow that represent fast and intermediate runoff and baseflow. These processes are implemented at the HRU level. For this, calculations about overland flow generation and soil moisture performed at the grid level are averaged over subwatersheds representing HRUs. Spatial arithmetic averaging soil water storage over all grid cells i contained within a given HRU j is represented using angle brackets $< . >$. The mass balance and percolation of water from the soil upper to the soil lower zone is implemented as:

$$Rech_j^t = < OVL_i^t >_j + < max(SM_i^t - FC_i, 0) >_j \tag{B.14}$$

$$SUZ_j^t = SUZ_j^{t-1} + Rech_j^t + Pond_j^t - Q0_j^t \Delta t - Q1_j \Delta t - PERC_j \tag{B.15}$$

$$SLZ_j^t = SLZ_j^{t-1} + PERC_j - Q2\Delta t \tag{B.16}$$

Rech (mm) is water storage in the near-surface compartment that generates fast runoff, SUZ (mm) is the storage in the upper groundwater compartment, and SLZ (mm) is water storage in the lower (deeper) groundwater compartment in HRU j at time step t. Q_0, Q_1, and Q_2 (mm d^{-1}) are specific runoff rates from the soil surface, and the upper and lower soil zones:

$$Q0_j^t = max((SUZ_j - HL1_j) * \frac{1}{CK0_j}, 0.0) \tag{B.17}$$

$$Q1_j^t = SUZ_j * \frac{1}{CK1_j} \tag{B.18}$$

$$Q2_j^t = SLZ_j * \frac{1}{CK2_j} \tag{B.19}$$

$$Qall_j^t = Q0_j^t + Q1_j^t + Q2_j^t \tag{B.20}$$

where $HL1$ (mm) is an empirical water storage threshold the triggers the generation of fast runoff, and $CK0$, $C10$, $CK2$ (d) are empirical parameters representing the characteristic drainage time of each of the compartments. Total outflow from HRU j on day t is distributed over time to produce the catchment response by convoluting the output of HRU j by triangular standard unit hydrograph with base M_{base}.

$$Q_j^t = \sum_{i=1}^{M_{base}} Qall_j^{t-i+1} U(i) \tag{B.21}$$

$$U(i) = \begin{cases} \frac{4}{M_{base}^2} * i & 0 < i < M_{base}/2 \\ -\frac{4}{M_{base}^2} * i + \frac{4}{M_{base}} & M_{base}/2 < i < M_{base} \end{cases} \tag{B.22}$$

where U is a triangular hydrograph of area 1 and a base $MAXBAS$ (d)representing the hydrograph duration .

B.0.2 Routing component

The response at the end of each HRU is routed through the stream network using the Muskingum-Cunge routing model. In this model the storage in each stream reach k is given by the following discharge-storage equation:

$$S_k^t = K \left[eQ_{in} + (1 - e)Q_{out} \right], \tag{B.23}$$

which has parameters K (d) and e (dimensionless) controlling, respectively, the celerity and dispersion of the wave routed through the channel.

Substituting this relationship in a finite-difference form of the continuity equation $\frac{S_j^{t+1} - S_j^t}{\Delta t} = Q_{in} - Q_{out}$ for a multi-reach system with lateral inflows injected upstream of reach draining HRU j at average constant rate through time step t q_j^{t+1} yields:

$$Q_j^{t+1} \left[K_j(1 - e_j) + 0.5\Delta t \right] + Q_{j-1}^{t+1} \left[K_j e_j - 0.5\Delta t \right] \tag{B.24}$$

$$= Q_j^t \left[K_j(1 - e_j) - 0.5\Delta t \right] + Q_{j-1}^t \left[K_j e_j + 0.5\Delta t \right] \tag{B.25}$$

$$+ q_j^{t+1} \left[K_j(1 - e_j) + 0.5\Delta t \right] \tag{B.26}$$

Each of the $HRUs$ contains one reach with an upstream and a downstream node. Streamflows for each of the $j = 1, ..., J$ reaches are integrated over time using a first-order explicit finite difference scheme. The system of J equations can be assembled as a linear system of the form:

$$\mathbf{A}\mathbf{Q^{t+1}} = \mathbf{B} \tag{B.27}$$

where $\mathbf{Q^{t+1}}$ is the vector of unknown streamflows at time $t + 1$ for each of the J reaches of the network that is solved each time step. Matrices $\mathbf{A}$ add $\mathbf{B}$ are functions

of the model parameters and streamflows at timestep t:

$$\mathbf{A} \equiv (\mathbf{a} + \mathbf{\Phi b})^T \tag{B.28}$$

$$\mathbf{B} \equiv (\mathbf{d} + \mathbf{\Phi c})^T \mathbf{Q}^t + \mathbf{I}(\mathbf{a} \odot \mathbf{q}^{t+1}) \tag{B.29}$$

where $\mathbf{\Phi}$ is a JxJ sparse connectivity (0,1)-matrix where the elements indicate if two pairs of nodes are connected. Flow direction is from nodes in the rows to nodes in the columns. Rows representing the upstream node of $HRUs$ that drain an outlet node (exit the domain) are all zero. Finally,

$$\mathbf{a} = \mathbf{I}(\mathbf{K} - \mathbf{K} \odot \mathbf{e}) + dt * 0.5 \tag{B.30}$$

$$\mathbf{b} = \mathbf{I}(\mathbf{K} \odot \mathbf{e}) - dt * 0.5 \tag{B.31}$$

$$\mathbf{c} = \mathbf{I}(\mathbf{K} - \mathbf{K} \odot \mathbf{e}) - dt * 0.5) \tag{B.32}$$

$$\mathbf{d} = \mathbf{I}(\mathbf{K} \odot \mathbf{e}) + dt * 0.5 \tag{B.33}$$

where $\mathbf{K}$ is the identity matrix of order J, $\mathbf{K}$ and $\mathbf{e}$ are column vectors holding parameters K and e for each of the N reaches in the network. The $\odot$ operator denotes the Schur (elementwise) product between two vectors. The solution of (B.27) becomes unstable if $\Delta t > 2 * K_j * (1 - e_j)$. To ensure robust and stable solution an adaptive time stepping scheme was implemented. In this scheme, the default time step is reduced by an integer fraction until the the stability condition is satisfied in all reaches.

Bibliography

[1] Jeffrey L. Anderson, Stephen L. Anderson, Jeffrey L. Anderson, and Stephen L. Anderson. A Monte Carlo Implementation of the Nonlinear Filtering Problem to Produce Ensemble Assimilations and Forecasts. *Monthly Weather Review*, 127(12):2741–2758, dec 1999.

[2] J. D. Annan, D. J. Lunt, J. C. Hargreaves, and P. J. Valdes. Parameter estimation in an atmospheric GCM using the Ensemble Kalman Filter. *Nonlinear Processes in Geophysics*, 12(3):363–371, feb 2005.

[3] S. Bergström. The HBV model - its structure and applications. *Swedish Meteorological and Hydrological Institute Reports Hydrology*, 1992.

[4] Sten Bergström. Development and Application of a Conceptual Runoff Model for Scandinavian Catchments. *Smhi*, 1976.

[5] M. Chen, S. Liu, L.L. Tieszen, and D.Y. Hollinger. An improved state-parameter analysis of ecosystem models using data assimilation. *Ecological Modelling*, 219(3-4):317–326, dec 2008.

[6] L.W Mays V.T Chow D.R Maidment. Unit Hydrograph. In *Applied Hydrology*. McGraw-Hill, New York, 1988.

[7] Geir Evensen. Sequential data assimilation with a nonlinear quasi-geostrophic model using Monte Carlo methods to forecast error statistics. *Journal of Geophysical Research*, 99(C5):10143, may 1994.

[8] Geir Evensen and Geir Evensen. Advanced Data Assimilation for Strongly Nonlinear Dynamics. *Monthly Weather Review*, 125(6):1342–1354, jun 1997.

[9] Andrew Gelman, John B. Carlin, Hal S. Stern, David B. Dunson, Aki Vehtari, Donald B. Rubin, John B. Carlin, Hal S. Stern, David B. Dunson, Aki Vehtari, and Donald B. Rubin. *Bayesian Data Analysis, Third Edition*. Chapman and Hall/CRC, nov 2018.

[10] H. J. Hendricks Franssen and W. Kinzelbach. Real-time groundwater flow modeling with the Ensemble Kalman Filter: Joint estimation of states and parameters and the filter inbreeding problem. *Water Resources Research*, 44(9), sep 2008.

[11] A. J. Jakeman and G. M. Hornberger. How much complexity is warranted in a rainfallâĂŘrunoff model? *Water Resources Research*, 1993.

[12] Andrew H. Jazwinski. Stochastic Processes and Filtering. *Mathematics in Science and Enginerring*, 1970.

[13] Simon J. Julier and Jeffrey K. Uhlmann. New extension of the Kalman filter to nonlinear systems. volume 3068, page 182. International Society for Optics and Photonics, jul 1997.

[14] R. E. Kalman. A New Approach to Linear Filtering and Prediction Problems. *Journal of Basic Engineering*, 82(1):35, mar 1960.

[15] Fang Liu and Fang Liu. Bayesian Time Series: Analysis Methods Using Simulation-Based Computation. 2000.

[16] Yuqiong Liu and Hoshin V. Gupta. Uncertainty in hydrologic modeling: Toward an integrated data assimilation framework. *Water Resources Research*, 43(7), jul 2007.

[17] Marco Maneta, Susanne Schnabel, and Victor Jetten. Continuous spatially distributed simulation of surface and subsurface hydrological processes in a small semiarid catchment. *Hydrological Processes*, 22(13):2196–2214, jun 2008.

[18] Stefano Mariani and Alberto Corigliano. Impact induced composite delamination: state and parameter identification via joint and dual extended Kalman filters. *Computer Methods in Applied Mechanics and Engineering*, 194(50-52):5242–5272, dec 2005.

[19] Robert N. Miller, Michael Ghil, and François Gauthiez. Advanced Data Assimilation in Strongly Nonlinear Dynamical Systems. *Journal of the Atmospheric Sciences*, 51(8):1037–1056, apr 1994.

[20] Rodolfo Alvarado Montero, Dirk Schwanenberg, Peter Krahe, and Peer Helmke. Unified Hydrological Flow Routing for Variational Data Assimilation and Model Predictive Control. In *Procedia Engineering*, volume 154, pages 1341–1348. Elsevier Ltd, 2016.

[21] Hamid Moradkhani, Soroosh Sorooshian, Hoshin V. Gupta, and Paul R. Houser. Dual state-parameter estimation of hydrological models using ensemble Kalman filter. *Advances in Water Resources*, 28(2):135–147, feb 2005.

[22] Jason W. Osborne. Advantages of hierarchical linear modeling. Osborne, Jason W. *Research & Evaluation*, 7(1), 2000.

[23] Rolf H. Reichle. Data assimilation methods in the Earth sciences. *Advances in Water Resources*, 31(11):1411–1418, nov 2008.

[24] Rolf H. Reichle, Dennis B. McLaughlin, Dara Entekhabi, Rolf H. Reichle, Dennis B. McLaughlin, and Dara Entekhabi. Hydrologic Data Assimilation with the Ensemble Kalman Filter. *Monthly Weather Review*, 130(1):103–114, jan 2002.

[25] Jan Seibert. Estimation of Parameter Uncertainty in the HBV Model. *Hydrology Research*, 28(4-5):247–262, aug 1997.

[26] Yuning Shi, Kenneth J. Davis, Fuqing Zhang, Christopher J. Duffy, and Xuan Yu. Parameter estimation of a physically based land surface hydrologic model using the ensemble Kalman filter: A synthetic experiment. *Water Resources Research*, 50(1):706–724, jan 2014.

[27] Soroosh Sorooshian and John A. Dracup. Stochastic parameter estimation procedures for hydrologie rainfall-runoff models: Correlated and heteroscedastic error cases. *Water Resources Research*, 16(2):430–442, apr 1980.

[28] Soroosh Sorooshian, Qingyun Duan, and Vijai Kumar Gupta. Calibration of rainfallâĂŘrunoff models: Application of global optimization to the Sacramento Soil Moisture Accounting Model. *Water Resources Research*, 29(4):1185–1194, apr 1993.

[29] Wood EF. Todini E, Szollosi-Nagy A. Adaptive stateâĂŞparameter estimation algorithm for real time hydrologic forecasting; a case study. *IISA/WMO Workshop on the Recent Developments in Real Time Forecasting/Control of Water Resources Systems*, 1976.

[30] Peter A. Troch, Claudio Paniconi, and Dennis McLaughlin. Catchment-scale hydrological modeling and data assimilation. *Advances in Water Resources*, 26(2):131–135, feb 2003.

[31] Jasper A. Vrugt, Cees G. H. Diks, Hoshin V. Gupta, Willem Bouten, and Jacobus M. Verstraten. Improved treatment of uncertainty in hydrologic modeling: Combining the strengths of global optimization and data assimilation. *Water Resources Research*, 41(1), jan 2005.

[32] Thorsten Wagener and Howard S. Wheater. Parameter estimation and regionalization for continuous rainfall-runoff models including uncertainty. *Journal of Hydrology*, 320(1-2):132–154, mar 2006.

[33] Markus Wallner, Uwe Haberlandt, and Jörg Dietrich. A one-step similarity approach for the regionalization of hydrological model parameters based on self-organizing maps. *Journal of Hydrology*, 2013.

[34] Xian-Huan Wen and Wen H. Chen. Real-Time Reservoir Model Updating Using Ensemble Kalman Filter With Confirming Option. *SPE Journal*, 11(04):431–442, dec 2006.

[35] Mike West. Mixture models, Monte Carlo, Bayesian updating, and dynamic models. *Computing Science and Statistics*, 1993.

[36] Mengsi Xiong, Pan Liu, Lei Cheng, Chao Deng, Ziling Gui, Xiaojing Zhang, and Yanghe Liu. Identifying time-varying hydrological model parameters to improve simulation efficiency by the ensemble Kalman filter: A joint assimilation of streamflow and actual evapotranspiration. *Journal of Hydrology*, 568:758–768, jan 2019.